



Sinter bonding and formation of a near-full-density bondline at 250 °C via addition of submicrometer Cu particles to micrometer Ag-coated Cu particles

Sung Yoon Kim¹ · Myeong In Kim¹ · Jong-Hyun Lee¹

Received: 17 June 2020 / Accepted: 10 August 2020 / Published online: 16 August 2020
© Springer Science+Business Media, LLC, part of Springer Nature 2020

Abstract

Pressure-assisted die bonding at 250 °C in air using a paste containing 2 μm Ag-coated Cu particles (Cu@Ag) and 350 nm Cu particles was demonstrated for power device bonding. At a Cu@Ag-to-Cu mixing ratio of 6:4, the sinter-bonded dies showed a considerable average shear strength that approached 25 MPa after only 5 min of bonding. Furthermore, a near-full-density bondline and excellent strength, greater than 30 MPa, were achieved after only 10 min. The remarkably rapid improvement in the strength and microstructure was attributed to the generation of pure Cu nanoparticles on the Cu surfaces by in situ reduction during heating for the bonding.

1 Introduction

With the continuous requirement for an increase in the efficiency of power-converting modules of hybrid and electronic vehicles, Si power devices are increasingly being replaced by wide-bandgap (WBG) semiconductor materials such as SiC and GaN [1–7]. A key characteristic of the materials used for high-end devices is the high power-converting efficiency at high temperatures. Insulated-gate bipolar transistor devices with higher power densities are also being developed [5–7]. To realize a die-bonding material with high heat endurance and conductance for assembling these devices, conventional high-Pb-bearing solders are being transferred to Ag, which is a representative alternative sinter-bonding material [8]. The melting temperature of Ag is significantly higher than 250–300 °C, which is believed to be the maximum chip temperature in WBG semiconductors; moreover, Ag has the highest thermal conductivity among metals.

Therefore, numerous sinter-bonding studies using pastes containing Ag particles have been conducted to develop alternative die-bonding technologies with or without the aid of external pressure [1, 2, 8–17]. However, the high material

cost and problem of Ag migration have resulted in studies using low-cost Cu-based materials that are similar in terms of conductivity [18–27]. Nevertheless, the development of processes targeting a reduction in the sintering time and temperature is also vital.

Sinter-bonding studies using pastes containing Cu particles, which provide the best compatibility with a Cu finish, generally require expensive processes involving inert or reducing atmospheres [18–26]. Because the particle size of Cu particles significantly influences the sintering speed, high-cost Cu nanoparticles have been used to increase the speed [19, 20, 22, 24, 25]. However, it is unproductive to use only nanoscale particles owing to the difficulty with mixing as well as increased material cost.

Herein, a high-speed die sinter-bonding method on a Cu finish is proposed at a relatively low temperature of 250 °C in air, using a low-cost Cu-particle-based material. The main particles employed were micrometer-sized Ag-coated Cu (Cu@Ag). The Ag shells in the particles are beneficial in suppressing the surface oxidation of Cu particles [28–30]. To prepare the sinter-bonding paste, 350 nm Cu particles were additionally incorporated into the paste to attain a high initial packing density and sinterability for rapid sintering and the formation of a near-full-density bondline under an external pressure.

✉ Jong-Hyun Lee
pljh@snut.ac.kr

¹ Department of Materials Science and Engineering,
Seoul National University of Science and Technology,
Seoul 01811, Republic of Korea

2 Materials and methods

2.1 Preparation of paste

Micrometer-sized Cu particles (average size: $\sim 2 \mu\text{m}$, JoinM) were coated with 20 wt% Ag shells via electroless plating, and the 350 nm Cu particles were synthesized in-house. These particles were mixed together at a specific particle-mixing ratio with a specially prepared reducing solvent to prepare the pastes. The weight ratio of the particle to solvent was fixed as 82:18.

2.2 Die bonding

Die bonding was performed using a dummy Cu die of area $3 \times 3 \text{ mm}^2$ on a dummy Cu substrate of area $10 \times 10 \text{ mm}^2$. The prepared paste was printed onto the substrates using a stencil containing a slit $3 \times 3 \times 0.1 \text{ mm}^3$ in volume. Subsequently, the die was aligned and placed on the printed pattern, and the sandwich-structured sample was heated in air up to $250 \text{ }^\circ\text{C}$ within 5 s and maintained at that temperature. Die bonding was performed under an external pressure of 10 MPa throughout the bonding time.

2.3 Characterization techniques

The initial morphologies of the prepared Cu@Ag and used Cu particles, the microstructures of the bondlines after sinter bonding, and the fracture surfaces after a shear test were examined by high-resolution scanning electron microscopy (HR-SEM, SU8010, Hitachi).

The bonding strength of a formed bondline, which was defined as the maximum stress measured during the shear test at a velocity of $200 \mu\text{m/s}$, was measured using a micro-bond tester (4000, Nordson DAGE). The height for shearing was $200 \mu\text{m}$ from the substrate surface.

Phase identification of the bondlines was conducted using X-ray diffraction (XRD, DE/D8 Advance, Bruker). The bondline surface was prepared for XRD by removing the total thickness of a chip and half thickness of a bondline via polishing after chip bonding in air. A Cu-finished alumina substrate was used with the sample for XRD measurement to confirm the existence of oxide peaks by reducing the intensities of the Cu peaks in the XRD results.

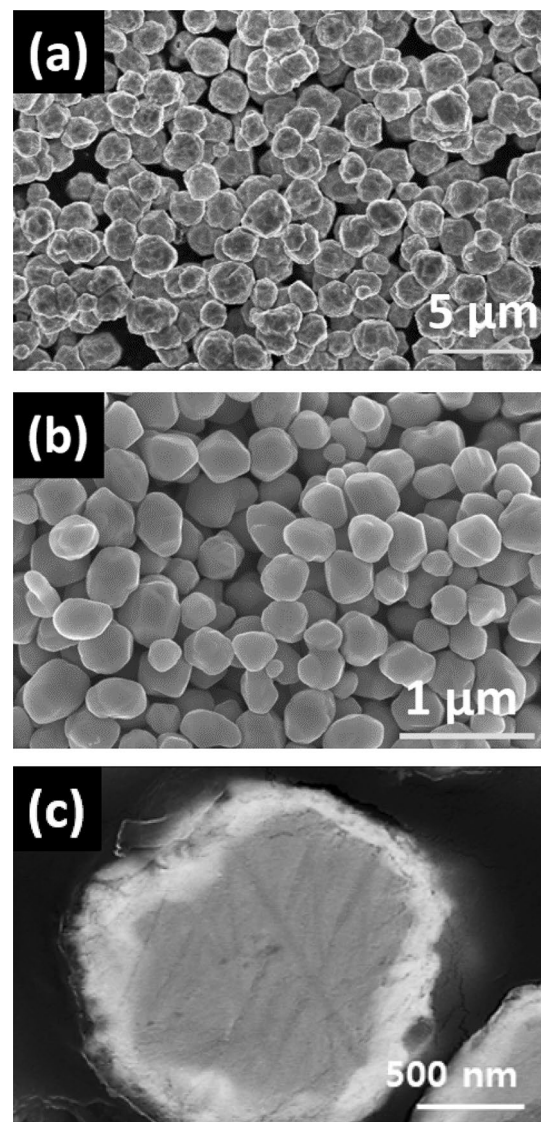


Fig. 1 SEM images of **a** the as-fabricated $2 \mu\text{m}$ Cu@Ag and **b** 350 nm Cu particles. **c** Cross-sectional back-scattered electron (BSE) image of the $2 \mu\text{m}$ Cu@Ag particle

3 Results and discussion

3.1 Used particles

The initial images of the used micrometer Cu@Ag and submicrometer Cu particles are shown in Fig. 1. The size and shape of the fabricated micrometer Cu@Ag ($\sim 2 \mu\text{m}$ and quasi-spherical shape) were not much different from those of the purchased core Cu particles owing to the thin Ag coating by the galvanic displacement reaction and electroless plating [29–31]. The average thickness of the Ag coating on a Cu@Ag particle was approximately 100 nm.

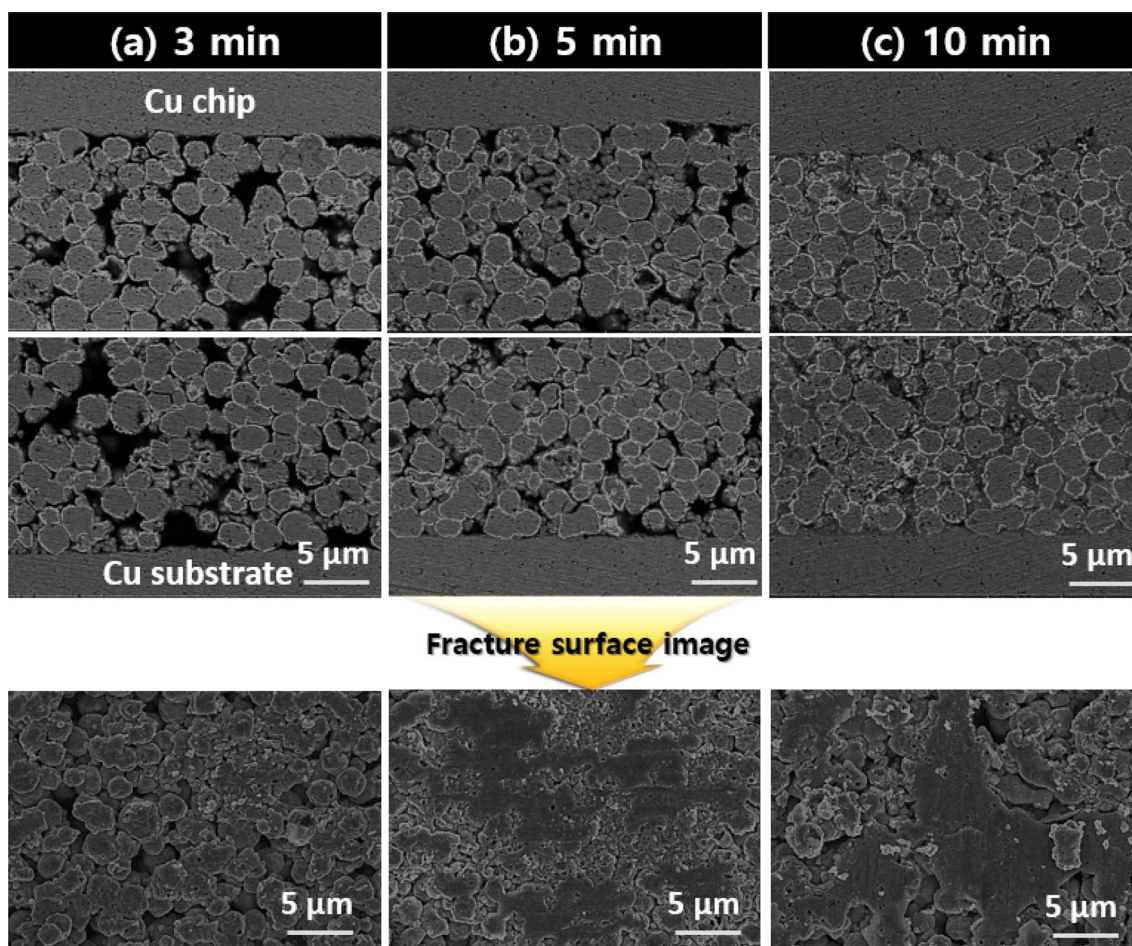


Fig. 2 Cross-sectional BSE images of the bondlines sinter-bonded for different bonding times at a mixing ratio of 8:2 and fracture surfaces: **a** 3, **b** 5, and **c** 10 min

The submicrometer Cu particles were approximately 350 nm in size, and presented a quasi-spherical shape.

3.2 Sinter-bonding properties

The microstructures of the bondlines sinter-bonded as a function of the mixing ratio and bonding time were observed. At the Cu@Ag-to-Cu mixing ratio of 8:2 (Fig. 2), the densities of the bondlines notably increased with an increase in the bonding time. This trend was also observed in the microstructures of the fracture surfaces; the degrees of sintering and densities of the fracture surfaces increased as the bonding time increased. All fractures occurred in patches in the vicinities of the chip/bondline and bondline/substrate interfaces across the bondline, indicating that the sintering was weakest around the interfaces.

When the mixing ratio was 6:4 (Fig. 3), the bondline densities at identical bonding times were enhanced owing to an increase in the degree of void filling by the 350 nm Cu particles. Hence, a near-full-density bondline was

eventually obtained in the 10-min-bonded sample, along with an increasing trend in the density with increasing bonding time. In the hard sphere model, the maximum packaging density is 74% [32]. However, the real maximum packaging density for monosized spherical particles can be significantly reduced depending on the method of packaging: 63–64% for random close packing [33, 34] and 55.0–55.5% for random loose packing [35]. Considering a bimodal size condition where the fraction of the 350 nm Cu particles was 40%, the maximum packing density is estimated to approach ~78% even in random loose packing and increase much more with external pressure [36]. Hence, the Cu particles in the sample contact most areas of both, the upper and lower interfaces, with increasing bonding time, as shown in Fig. 3c. Evidently, the densities of the fracture surfaces at an identical bonding time were also improved compared to those at a mixing ratio of 8:2. All fractures were observed in patches around the upper and lower interfaces across the bondline.

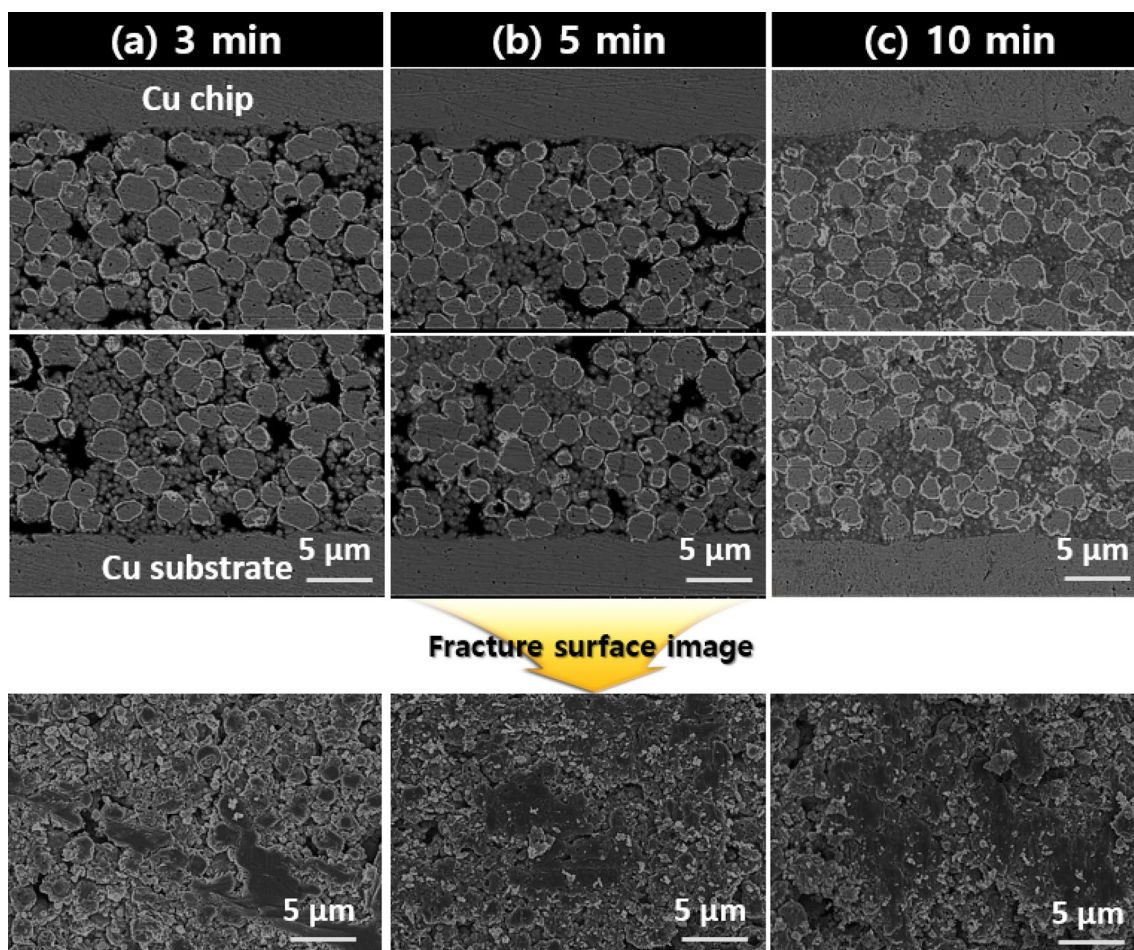


Fig. 3 Cross-sectional BSE images of the bondlines sinter-bonded for different bonding times at a mixing ratio of 6:4 and fracture surfaces: **a** 3, **b** 5, and **c** 10 min

3.3 Sinter-bonding mechanism

The preferential sintering among the 2 μm Cu@Ag particles can be explained by the dewetting behavior of the Ag shells in the Cu@Ag particles, which occurred as the temperature approached 250 $^{\circ}\text{C}$ via the interfacial instability induced by a lattice mismatch of 11.7% between Ag and Cu [37]. The Ag dewetted from the nanoscale nodules can rapidly sinter with other Ag nodules on neighboring Cu@Ag particles when the Cu@Ag particles are in contact. Note that sintering between the Cu@Ag particles occurred even in the 1-min-bonded samples. Subsequently, Ag necking was followed by Cu necking [29, 38]. The Cu from the cores diffused across the cores through the connected Ag nodules with an increase in the bonding time, resulting in stronger sintering between the Cu cores [29]. The out-diffused Cu can sinter-bond with the slightly oxidized Cu finish by virtue of the reducibility of the solvent used in the paste until it evaporates. However, all the microstructures indicate the occurrence

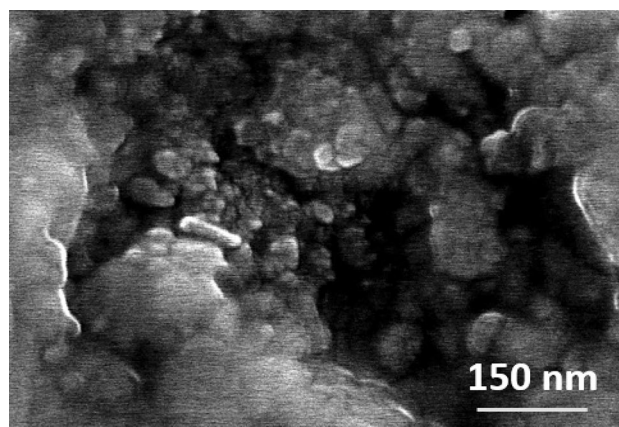


Fig. 4 Enlarged SEM image showing the bondline of the Fig. 3b sample

of incomplete sintering, because the size and proportion of the interparticulate voids and particle–interface voids are significant.

With the inclusion of the 350 nm Cu particles, the oxide layers on the surface of the Cu particles can also be reduced with the help of a reducing solvent, resulting in the formation of in situ small and pure Cu nanoparticles, as shown in Fig. 4. The generated Cu nanoparticles may behave transiently like a quasi-fluid via the melting-point depression phenomenon due to the Gibbs–Thomson effect [39–42]. Thus, 350 nm Cu particles with the generated Cu nanoparticles can easily be sintered with every neighboring material, such as Cu@Ag particles, 350 nm Cu particles, and Cu finishes. The Cu nanoparticles generated from the 350 nm Cu particles and Cu finishes are highly useful as sintering accelerators owing to their high surface area and activity [19, 20, 22, 24, 25]. Following Ag dewetting, the 350 nm Cu particles can contact and sinter with the exposed Cu diffused out through the thin Ag layer between the formed Ag nodules, which results in stronger connection. The transformation to a near-full-density structure from 5 min (Fig. 3b) to 10 min (Fig. 3c) might be attributed to the greater compactness and contact by rearrangement, whereby the particles are packed down during continual pressing due to bonding.

Based on different phenomena, the sequential mechanism for the rapid sinter bonding and formation of the near-full-density bondline is shown in Fig. 5. First, the Ag shells were dewetted and transformed into a nodular shape on

the micrometer Cu particles during heating. The nanoscale nodules rapidly sintered with other nodules, forming necks between the Ag nodules. However, the sintering degree in this state was low. Subsequently, the oxide layers on the surfaces of the 350 nm Cu particles were reduced and transformed into pure Cu nanoparticles. The Cu nanoparticles rapidly sintered with the other Cu nanoparticles and Cu finishes due to their transient quasi-fluid behaviors. In addition, the micrometer Cu cores sintered with the other Cu cores via the out-diffusion of Cu through the sintered Ag nodules. The diffused Cu also sintered with the 350 nm Cu particles and Cu finishes. These extensive sintering events at all the contacts enhanced the solidity of the bondline. The different sintering events were intensified by the enlarged sintering areas at the contacts with increasing bonding time, to ultimately provide adequate strength to the bondline. Consequently, the bondline gradually transformed into a near-full-density structure without particulate voids via continuous particle rearrangement under the pressure during bonding.

3.4 Bonding strength

Figure 6 shows the shear strength of the Cu dummy dies sinter-bonded at 250 °C as a function of the mixing ratio and bonding time. The bondlines by single-modal Cu@Ag

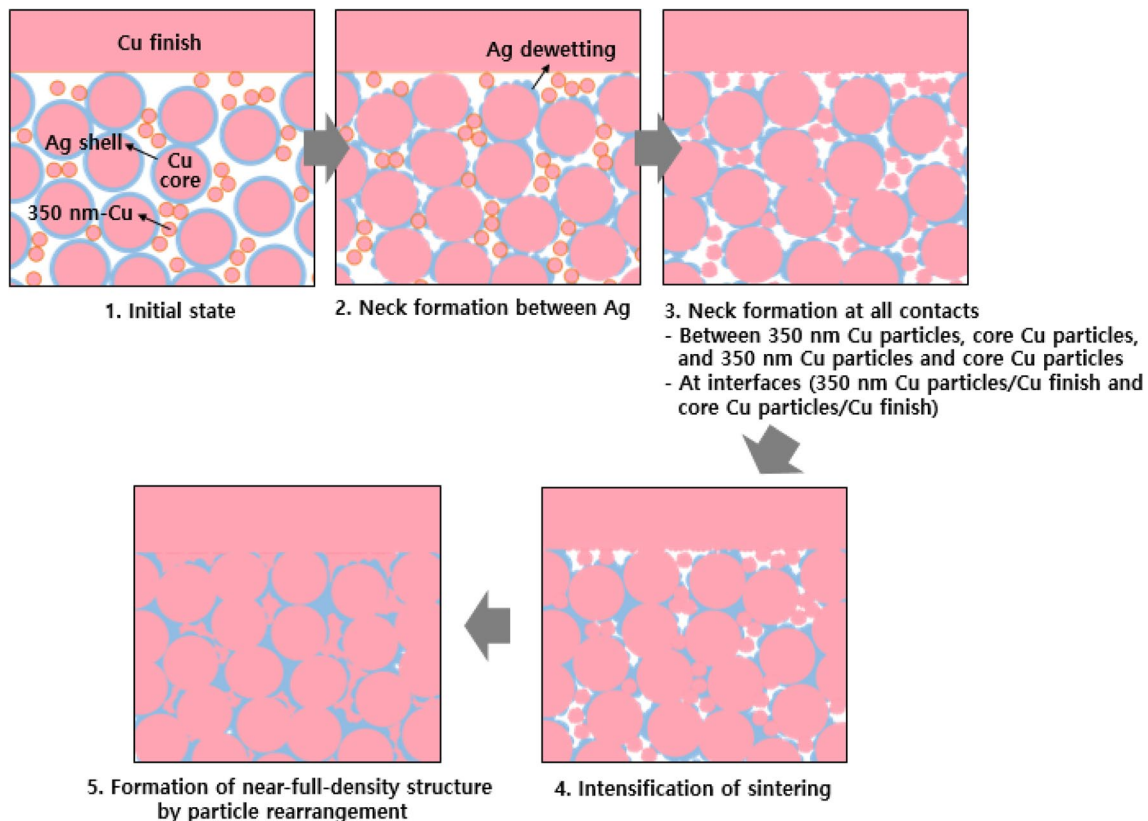


Fig. 5 Mechanism of rapid sinter bonding and formation of the near-full-density bondline

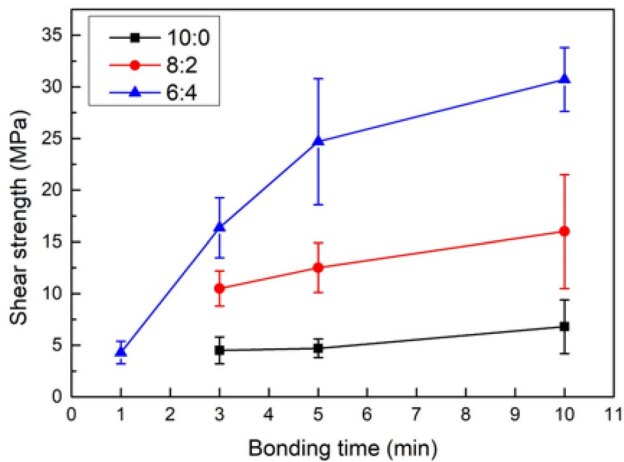


Fig. 6 Shear strength of a Cu dummy die sinter-bonded at 250 °C in air at different mixing ratios and bonding times

particles (10:0) exhibited the lowest shear strengths, and the strength increase was insignificant as the bonding time increased. Meanwhile, the bondlines by bimodal particles showed a pronounced strength increase with an increase in bonding time. In particular, the 6:4 sample showed the highest strength and greatest increase trend. As a representative result, excellent shear strengths approaching 25 MPa and exceeding 30 MPa were measured after short durations of 5 and 10 min, respectively, both of which are much higher than that of a die attached using a Pb–5Sn solder [43]. The adequate shear strength and near-full-density structure were realized remarkably rapidly compared to prior studies employing similar conditions and Ag bimodal particles [9, 14].

The increasing trend observed as a function of bonding time in the bimodal pastes can be explained by the stronger sintering at the interfaces and among the particles. The weakened strength increase with an increase in bonding

time at a mixing ratio of 8:2 is attributed to inadequate sintering at the chip/bondline and bondline/substrate interfaces, as well as between the micrometer Cu@Ag particles due to the insufficient amount of 350 nm Cu particles.

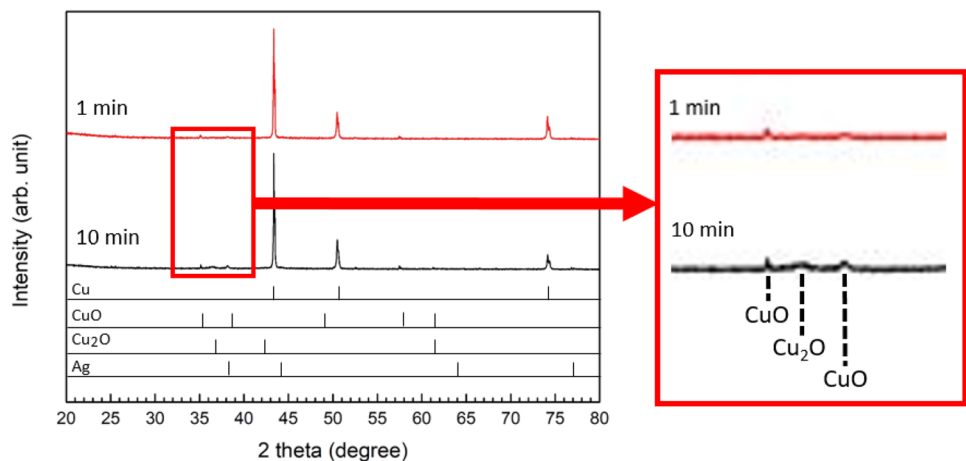
3.5 Suppressed oxidation in a bondline

XRD results of the 6:4 samples air-annealed at 250 °C for a specific time are shown in Fig. 7. In the 1-min-bonded sample, only a trace CuO phase was detected, which can be understood as oxidation in the copper exposed to air after evaporation of the reducing solvent. Meanwhile, a small peak of the Cu₂O phase was also observed along with increased CuO peaks in the 10-min-bonded sample, which implies the continuation of oxidation via longer sintering in air. However, even the additional oxidation was insignificant because the compactness of the bondline significantly increased during the sinter bonding. In conclusion, the Ag shells were beneficial in suppressing the oxidation of the large-volume micrometer Cu particles for heating in air, enabling excellent thermal conduction through the bondline.

3.6 Improvements over previous bonding methods

This facile die-bonding method can simultaneously overcome the limitations of prior studies that used pure Ag particles (high material cost, high bonding temperature, long bonding time, and low compatibility with a low-cost Cu finish) as well as those that used pure Cu particles (requirement of an inert or reducing atmosphere, high bonding temperature, long bonding time, and nanoparticle-based filler material). Hence, it is remarkably competitive for attaching WBG power devices.

Fig. 7 XRD patterns of samples air-annealed at 250 °C for different times at a Cu@Ag-to-Cu mixing ratio of 6:4



4 Conclusions

Die sinter bonding in air using 2 μm Cu@Ag/350 nm Cu bimodal particles was successfully demonstrated. The mixing ratio of the 2 μm Cu@Ag and 350 nm Cu particles was a crucial factor for the sinter bondability, and excellent bonding results were obtained at a ratio of 6:4; excellent shear strengths approaching 25 MPa and surpassing 30 MPa were measured even after rapid sinter bonding for only 5 and 10 min, respectively. Moreover, the near-full-density structure observed in the bondline formed for 10 min corresponded well with the excellent strength. The observed sinter-bonding speed has seldom been reported even in similar studies using micrometer Ag particle-based pastes. The remarkably rapid improvement in the strength and microstructure was mainly attributed to the production of small pure Cu nanoparticles on the 350 nm Cu surfaces via in situ reduction during heating. Furthermore, the degrees of oxidation in the formed bondlines were insignificant.

Acknowledgements This work was supported by a Korea Institute for Advancement of Technology (KIAT) grant funded by the Korea Government (MOTIE) (P0002092, The Competency Development Program for Industry Specialist).

References

- H.S. Chin, K.Y. Cheong, A.B. Ismail, A review on die attach materials for SiC-based high-temperature power devices. *Metall. Mater. Trans. B* **41**, 824–832 (2010)
- A. Drevin-Bazin, F. Lacroix, J.F. Barbot, SiC die attach for high-temperature applications. *J. Electron. Mater.* **43**, 695–701 (2014)
- T. Kimoto, H. Niwa, T. Okuda, E. Saito, Y. Zhao, S. Asada, J. Suda, Carrier lifetime and breakdown phenomena in SiC power device material. *J. Phys. D: Appl. Phys.* **51**, 363001 (2018)
- J. Hu, Y. Zhang, M. Sun, D. Piedra, N. Chowdhury, T. Palacios, Materials and processing issues in vertical GaN power electronics. *Mater. Sci. Semicond. Proc.* **78**, 75–84 (2018)
- T.-C. Chang, C.-C. Lee, C.-P. Hsieh, S.-C. Hung, R.-S. Cheng, Electrical characteristics and reliability performance of IGBT power device packaging by chip embedding technology. *Microelectron. Reliab.* **55**, 2582–2588 (2015)
- L. Ceccarelli, P.D. Reigosa, F. Iannuzzo, F. Blaabjerg, A survey of SiC power MOSFETs short-circuit robustness and failure mode analysis. *Microelectron. Reliab.* **76–77**, 272–276 (2017)
- L.-L. Li, Z.-F. Liu, M.-L. Tseng, L. Zhou, F.-D. Qi, Prediction of IGBT power module remaining lifetime using the aging state approach. *Microelectron. Reliab.* **102**, 113476 (2019)
- K.S. Siow, Y.T. Lin, Identifying the development state of sintered silver (Ag) as a bonding material in the microelectronic packaging via a patent landscape study. *J. Electron. Packag.* **138**, 020804 (2016)
- K. Suganuma, S. Sakamoto, N. Kagami, D. Wakuda, K.-S. Kim, M. Nogi, Low-temperature low-pressure die attach with hybrid silver particle paste. *Microelectron. Reliab.* **52**, 375–380 (2012)
- S. Wang, H. Ji, M. Li, C. Wang, Fabrication of interconnects using pressureless low temperature sintered Ag nanoparticles. *Mater. Lett.* **85**, 61–63 (2012)
- J. Yan, G. Zou, A. Wu, J. Ren, J. Yan, A. Hu, Y. Zhou, Pressureless bonding process using Ag nanoparticle paste for flexible electronics packaging. *Scr. Mater.* **66**, 582–585 (2012)
- S. Soich, K. Suganuma, Low-temperature and low-pressure die bonding using thin Ag-flake and Ag-particle pastes for power device. *IEEE Trans. Compon. Packag. Technol.* **3**, 923–929 (2013)
- S. Fu, Y. Mei, G.-Q. Lu, X. Li, G. Chen, X. Chen, Pressureless sintering of nanosilver paste at low temperature to join large area ($\geq 100 \text{ mm}^2$) power chips for electronic packaging. *Mater. Lett.* **128**, 42–45 (2014)
- J. Jiu, H. Zhang, S. Nagao, T. Sugahara, N. Kagami, Y. Suzuki, Y. Akai, K. Suganuma, Die-attaching silver paste based on a novel solvent for high-power semiconductor devices. *J. Mater. Sci.* **51**, 3422–3430 (2016)
- H. Zhang, C. Chen, J. Jiu, S. Nagao, K. Suganuma, C. Chen, K. Suganuma, High-temperature reliability of low-temperature and pressureless micron Ag sintered joints for die attachment in high-power device. *J. Mater. Sci.: Mater. Electron.* **29**, 8854–8862 (2018)
- J. Li, X. Li, L. Wang, Y.-H. Mei, G.-Q. Lu, A novel multiscale silver paste for die bonding on bare copper by low-temperature pressure-free sintering in air. *Mater. Des.* **140**, 64–72 (2018)
- Z. Zhang, C. Chen, Y. Yang, H. Zhang, D. Kim, T. Sugahara, S. Nagao, K. Suganuma, Low-temperature and pressureless sinter joining of Cu with micron/submicron Ag particle paste in air. *J. Alloys Compd.* **780**, 435–442 (2019)
- X. Liu, H. Nishikawa, Low-pressure Cu-Cu bonding using in-situ surface-modified microscale Cu particles for power device packaging. *Scr. Mater.* **120**, 80–84 (2016)
- J. Liu, H. Chen, H. Ji, M. Li, Highly conductive Cu–Cu joint formation by low-temperature sintering of formic acid-treated Cu nanoparticles. *ACS Appl. Mater. Interfaces* **8**, 33289–33298 (2016)
- J. Li, X. Yu, T. Shi, C. Cheng, J. Fan, S. Cheng, G. Liao, Z. Tang, Low-temperature and low-pressure Cu–Cu bonding by highly sinterable Cu nanoparticle paste. *Nanoscale Res. Lett.* **12**, 255 (2012)
- Y. Gao, H. Zhang, W. Li, J. Jiu, S. Nagao, T. Sugahara, K. Suganuma, Die bonding performance using bimodal Cu particle paste under different sintering atmospheres. *J. Electron. Mater.* **46**, 4575–4581 (2017)
- Y. Mou, Y. Peng, Y. Zhang, H. Cheng, M. Chen, Cu-Cu bonding enhancement at low temperature by using carboxylic acid surface-modified Cu nanoparticles. *Mater. Lett.* **227**, 179–183 (2018)
- Y. Gao, W. Li, H. Zhang, J. Jiu, D. Hu, K. Suganuma, Size-controllable synthesis of bimodal Cu particles by polyol method and their application in die bonding for power devices. *IEEE Trans. Compon. Packag. Manufact. Technol.* **8**, 2190–2197 (2018)
- Y. Kamikoriyama, H. Imamura, A. Muramatsu, K. Kanie, Ambient aqueous-phase synthesis of copper nanoparticles and nanopastes with low-temperature sintering and ultra-high bonding abilities. *Sci. Rep.* **9**, 899 (2019)
- J. Li, Q. Liang, T. Shi, J. Fan, B. Gong, C. Feng, J. Fan, G. Liao, Z. Tang, Design of Cu nanoaggregates composed of ultra-small Cu nanoparticles for Cu-Cu thermocompression bonding. *J. Alloys Compd.* **772**, 793–800 (2019)
- R. Gao, S. He, Y.-A. Shen, H. Nishikawa, Effect of substrates on fracture mechanism and process optimization of oxidation–reduction bonding with copper microparticles. *J. Electron. Mater.* **48**, 2263–2271 (2019)
- W.L. Choi, Y.S. Kim, K.-S. Lee, J.-H. Lee, Characterization of the die-attach process via low-temperature reduction of Cu formate in air. *J. Mater. Sci.: Mater. Electron.* **30**, 9806–9813 (2019)
- X. Xu, X. Luo, H. Zhuang, W. Li, B. Zhang, Electroless silver coating on fine copper powder and its effects on oxidation resistance. *Mater. Lett.* **57**, 3987–3991 (2003)

29. C.H. Lee, E.B. Choi, J.-H. Lee, Characterization of novel high-speed die attachment method at 225 °C using submicrometer Ag-coated Cu particles. *Scr. Mater.* **150**, 7–12 (2018)
30. E.B. Choi, J.-H. Lee, Submicron Ag-coated Cu particles and characterization methods to evaluate their quality. *J. Alloys Compd.* **689**, 952–958 (2016)
31. E.B. Choi, J.-H. Lee, Dewetting behavior of Ag in Ag-coated Cu particle with thick Ag shell. *Appl. Surf. Sci.* **480**, 839–845 (2019)
32. E. Dickinson, Statistical model of a suspension of deformable particles. *Phys. Rev. Lett.* **53**, 728 (1984)
33. A.R. Kansal, S. Torquato, F.H. Stillinger, Diversity of order and densities in jammed hard-particle packings. *Phys. Rev. E* **66**, 041109 (2002)
34. A.R. Kansal, S. Torquato, F.H. Stillinger, Computer generation of dense polydisperse sphere packings. *J. Chem. Phys.* **117**, 8212–8218 (2002)
35. G.Y. Onoda, E.G. Liniger, Random loose packings of uniform spheres and the dilatancy onset. *Phys. Rev. Lett.* **64**, 2727–2730 (1990)
36. H.J.H. Brouwers, Particle-size distribution and packing fraction of geometric random packings. *Phys. Rev. E* **74**, 031309 (2006)
37. M. Grouchko, A. Kamyshny, S. Magdassi, Formation of air-stable copper–silver core–shell nanoparticles for inkjet printing. *J. Mater. Chem.* **19**, 3057–3062 (2009)
38. X. Yu, J. Li, T. Shi, C. Cheng, G. Liao, J. Fan, T. Li, Z. Tang, A green approach of synthesizing of Cu-Ag core-shell nanoparticles and their sintering behavior for printed electronics. *J. Alloys Compd.* **724**, 365–372 (2017)
39. M. Takagi, Electron-diffraction study of liquid-solid transition of thin metal films. *J. Phys. Soc. Jpn.* **9**, 359–363 (1954)
40. P.R. Couchman, W.A. Jesser, Thermodynamic theory of size dependence of melting temperature in metals. *Nature* **269**, 481 (1977)
41. G.L. Allen, R.A. Bayles, W.W. Jesser, Small particle melting of pure metals. *Thin Solid Films* **144**, 297–308 (1986)
42. T. Liang, D. Zhou, Z. Wu, P. Shi, Size-dependent melting modes and behaviors of Ag nanoparticles: a molecular dynamics study. *Nanotechnology* **28**, 485704 (2017)
43. K. Suganuma, S.-J. Kim, K.-S. Kim, *JOM* **61–71**, 64 (2009)

Publisher's Note Springer Nature remains neutral with regard to jurisdictional claims in published maps and institutional affiliations.